Experimental Insight into the Hemodynamics and Perfusion of Radiological Contrast in Patent and Non-patent Aortic Dissection Models

Elie Salameh,[1] Charbel Saade,[2] and Ghanem F. Oweis [ID][1]

[1]Department of Mechanical Engineering, M.S. Faculty of Engineering & Architecture, American University of Beirut, PO Box 11-0236, Beirut 1107-2020, Lebanon; and [2]Medical Imaging Sciences, Faculty of Health Sciences, American University of Beirut, PO Box 11-0236, Beirut 1107-2020, Lebanon

Associate Editor Ajit P. Yoganathan oversaw the review of this article.

Abstract—*Purpose*—In a curved vessel such as the aortic arch, the velocity profile closer to the aortic root is normally skewed towards the inner curvature wall, while further downstream along the curve, the velocity profile becomes skewed towards the outer wall. In an aortic dissection (AD) disease, blood velocities in the true lumen (TL) and false lumen (FL) are hypothesized to depend on the proximity of the entry tear to the root of aortic arch. Faster velocity in the FL can lead to higher hemodynamic loading, and pose tearing risk. Furthermore, the luminal velocities control the perfusion rate of radiological contrast media during diagnostic imaging. The objective in this study is to investigate the effect of AD disease morphology and configuration on the blood velocity field in the TL and FL, and on the relative perfusion of radiological enhancement agents through the dissection.
Methods—Eight *in vitro* models were studied, including patent and non-patent FL configurations. Particle image velocimetry (PIV) was used to quantify the AD velocity field, while laser-induced fluorescence (LIF) was implemented to visualize dynamical flow phenomena and to quantify the perfusion of injected dye, in mimicry of contrast-enhanced computed tomography (CT).
Results—The location of the proximal entry tear along the aortic arch in a patent FL had a dramatic impact on whether the blood velocity was higher in the TL or FL. The luminal velocities were dependent on the entry/reentry tear size combination, with the smaller tear (whether distal or proximal) setting the upper limit on the maximal flow velocity in the FL. Upon merging near the distal reentry tear, the TL/FL velocity differential gave rise to the roll up and shedding of shear layer vortices that convected downstream in close proximity to the wall of the non-dissected aorta. In a non-patent FL, the flow velocity was practically null with all the blood passing through the TL. LIF imaging showed much slower perfusion of contrast dye in the FL compared to the TL. In a patent FL, however, dye had a comparable perfusion rate appearing around the same time as in the TL.
Conclusions—Blood velocities in the TL and FL were highly sensitive to the exact dissection configuration. Geometric case A1R, which had its proximal entry tear located further downstream along the aortic arch, and had its entry and reentry tears sufficiently sized, exhibited the highest FL flow velocity among the tested models, and it was also higher than in the TL, which suggest that this configuration had elevated hemodynamic loading and risk for tearing. In contrast-enhanced diagnostic imaging, a time-delayed acquisition protocol is recommended to improve the detection of suspected cases with a non-patent FL.

Keywords—Patent false lumen, Stanford type A, PIV, LIF, Shear layer vortex, Contrast computed X-ray tomography (CT), Magnetic resonance (MR), Tear propagation.

INTRODUCTION

Aortic dissection (AD) is an uncommon, but fatal, abnormality of the aorta with an estimated annual incidence of 30 new cases per million.[19,54] Tearing and delamination of the diseased vessel's intimal wall layer creates two parallel blood conduits: true lumen (TL) and false lumen (FL).[19,60] The *intimal flap*, or the septum separating the two lumina, may flutter with the cardiac cycle,[8,18] or it can be stiff in chronic fibrosed cases.[59] Blood exchange between the TL and FL occurs through *entry tears* and *reentry tears*. Depending on the number and tear configuration the FL flow can be *patent* or *non-patent* (occluded).

The morphological configuration of AD forms the basis for clinical assessment and prognosis. For example, the diameter of the dilated aorta has been used broadly as an indicator of disease progression.[17,20,39,50,58] A patent FL flow can signify an ad-

Address correspondence to Ghanem F. Oweis, Department of Mechanical Engineering, M.S. Faculty of Engineering & Architecture, American University of Beirut, PO Box 11-0236, Beirut 1107-2020, Lebanon. Electronic mail: goweis@aub.edu.lb

vanced disease stage, and is thought to portend high mortality risk. Complete thrombosis of the FL is often viewed favorably, while partial thrombosis involves the risk of clot detachment and breakup. The number of tears, their geometrical configuration, and size details are related to disease severity and prognosis.[3,17,50,53,59]

Disease morphology plays a critical role in its hemodynamics, which consequently affects disease remodeling and progression, and prognosis. *In-vitro*[7,50,59] and in silico AD models[1,3,29,48,53,55] have been proffered to understand the AD hemodynamics. The effect of tear configuration and size have been shown[3,17,50,53,59] to impact the FL pressure. Flow reversal in the complaint AD[7] is a particular occurrence that can significantly alter the wall shear stress magnitude and direction. Swirling flow structures were also found in rigid computational model of the disease.[1]

Hemodynamics fundamentally impact the diagnostic imaging of AD, particularly, *contrast-enhanced* magnetic resonance MR,[14,39] and *contrast* X-ray computed tomography CT.[2,21,42,43] The contrast media is injected into the peripheral venous system (typically the arm) and carried by the blood stream to enhance the aorta in the radiographs. Elevated volume and rate of injection are necessary to allow sufficient media to reach the aorta.[30,42,52] Precise injection and image acquisition timing are employed for better diagnostics, and for tighter control of the nephrotoxic contrast volume.[36,51,62] Flow dynamics in the complex AD geometry[12,24,27,28,61] impact contrast mixing and transport and subsequently affect the nature and interpretation of the resulting angiogram. Incorrect AD diagnosis, whether false positive or false negative, is not uncommon.[5,21,25,33,34,35,44,45,47] This is related to the complex nature of the anatomy and hemodynamics, scanner capabilities, and—not the least—staff training and experience.[47,52,54] The challenge is compounded by the need for a quick diagnosis[42]: the risk of in-hospital mortality increases at an average rate of 1% per hour in the first day.[54]

The underlying quantity that sets the hemodynamic forcing on the vessel is the velocity field. Proximally in a non-dissected curved vessel, the faster velocity is skewed towards the inner curvature wall.[22] Further downstream along the bend, the faster velocity becomes skewed towards the outer wall of the curved vessel[4] due to the centripetal 3-D flow effects.[22] It is hypothesized that proximity to the aortic root of the entry tear is a critical parameter in whether the faster flow velocity develops in the TL or in the patent FL. A faster FL flow implies higher biomechanical loading and risk for tear expansion and disease progression.

In this paper eight patent and non-patent AD geometric models are tested *in vitro* to measure changes in TL and FL flow velocities with changes in the underlying dissection geometry. These models are further tested using surrogate contrast-injection diagnostic imaging to elucidate the effect of FL patency on the nature of the acquired diagnostic images and protocols. Flow velocities are measured using particle image velocimetry (PIV). The optical imaging method laser induced fluorescence (LIF) is used as a proxy for contrast-CT imaging to measure and visualize the perfusion of contrast dye in the dissection.

METHODS

Plexiglass phantom models of the aortic dissection (AD) were connected to a continuous flow circulatory system with water as blood surrogate. Laser-assisted PIV and LIF optical imaging measurements were obtained in the transparent models to quantify the flow velocities in the TL and FL, and to visualize the transport dynamics of the injected contrast media analog. A schematic of the experiment is shown in Fig. 1.

Dissection Models and Flow Loop

The aortic arch was modeled with a square-cross-section of 14 mm side length at its proximal and distal ends, and it had a planar bend of 35 mm radius of curvature[4] measured at the aorta's inner wall. Two AD models denoted here as A and B and shown in Fig. 2 were cut and machined from an optically clear plexiglass sheet 20 mm thick, and their surfaces were hand polished inside out. In both models, the dissection started in the ascending aorta. A 4 mm thick plexiglass plate was glued using clear polyurethane liquid as a top cover, and inlet and outlet pipe-fittings were installed and connected to a submersible centrifugal pump (5 W) in a ~ 6 L water reservoir approximating the total blood volume in the body. The continuous pump produced a steady bulk flow rate of 3 *l/min*, which varied by less than 5% across all geometric models. This was consistent with the flow rate computed from sectional PIV velocity profiles. The cross-sectional inlet velocity profile was allowed to develop naturally in the connecting tubes and the model. It was measured directly with PIV in the straight inlet part of the model and could be approximately fitted with a parabolic distribution. The inlet Reynolds number based on the hydraulic diameter of the square duct (D_h = 14 mm) was Re = 3787, and this was close to reported values for the aorta of Re = 4000,[32] and near peak-systole aortic Re range of 4200–6100.[16] In a study of the
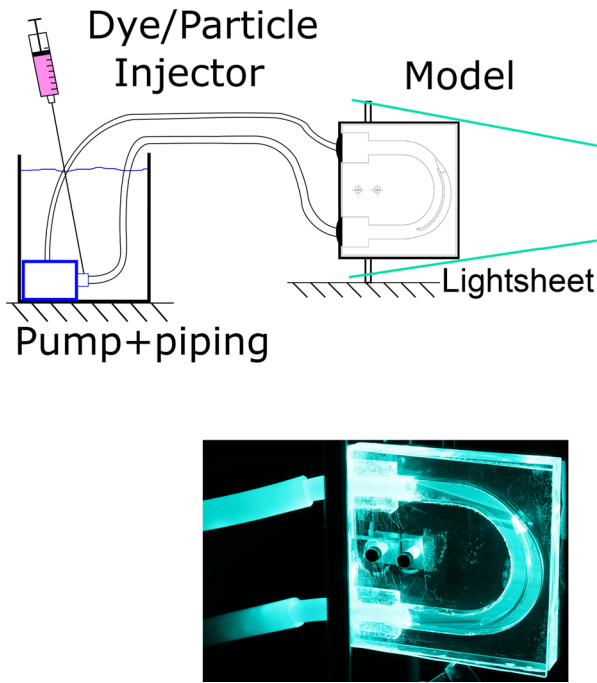
FIGURE 1. (Top) Schematic of the AD flow loop and optical imaging measurement setup used in both PIV and LIF. The discharge pipe outlet and the pump's inlet were placed at opposite corners in the container (~ 10 cm apart) to allow for dye dilution by mixing. The 5 mL dye injector was actuated manually. (Bottom) A picture of one optically clear AD model installed in the test setup and illuminated by the laser sheet.

periodic flow in a bend[49] the systolic part of the cycle was found to be more important in controlling the energetic flow dynamics than the diastolic part. The planar aorta and its square shape were necessary simplifications to minimize optical distortions in the PIV and LIF measurements without recourse to more costly refractive index matching fluids.[4] Common index-matching fluids have a density close to the iodinated radiological contrast agent, and that was an undesirable option since a future objective was to maintain the density difference between the blood surrogate and radiological contrast. The square geometry has been adopted previously for its flat imaging area to study the flow in an aortic arch.[31] The A & B models had a patent FL, with one of the tears differently sized than in the other model. To mimic the scenario of a non-patent AD, for instance from a blocking clot, a small piece of optically clear RTV rubber was selected to jam one tear. To mimic the scenario when the flap at the proximal or distal tears fluttered *into* the main blood streams,[7] a rigid and stationary geometric flutter feature was incorporated in the model. By reversing the model's inlet and outlet connections the number of geometric cases was doubled from four to eight allowing the study of the effects of placement of the dissected flap, and of tear size
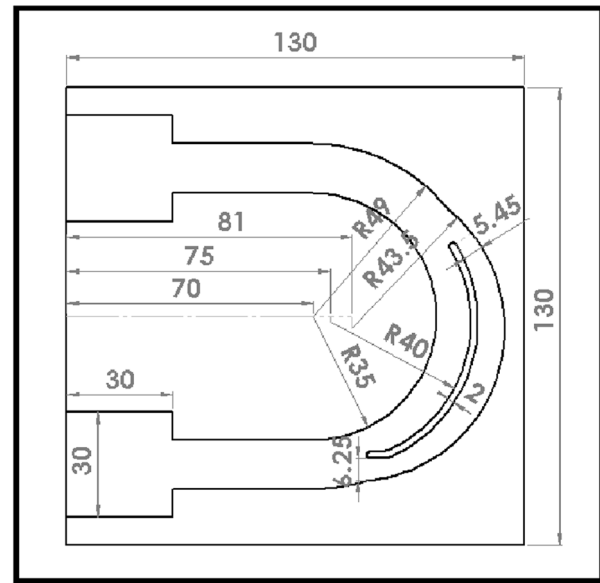
Model A
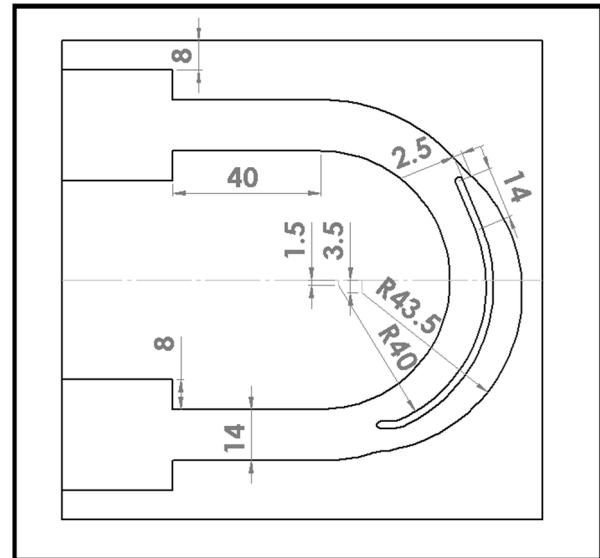
Model B

FIGURE 2. Dimensioned drawings in (mm) of the two manufactured AD models A and B. The aortic channel has uniform 14 mm depth into the page.

configurations. Eight different disease geometric case scenarios were investigated in total: four with a *patent FL* shown in Fig. 3a, and four with a *non-patent FL* shown in Fig 3b. The 8 case scenarios summarized in Table 1 were labeled by concatenating three characters according to: (i) the model used (A or B); (ii) whether it was patent or non-patent (1 or 2); and (iii) whether the *stationary* flutter feature was proximal or distal (F or R). So for example, scenario B2R used model (B), was
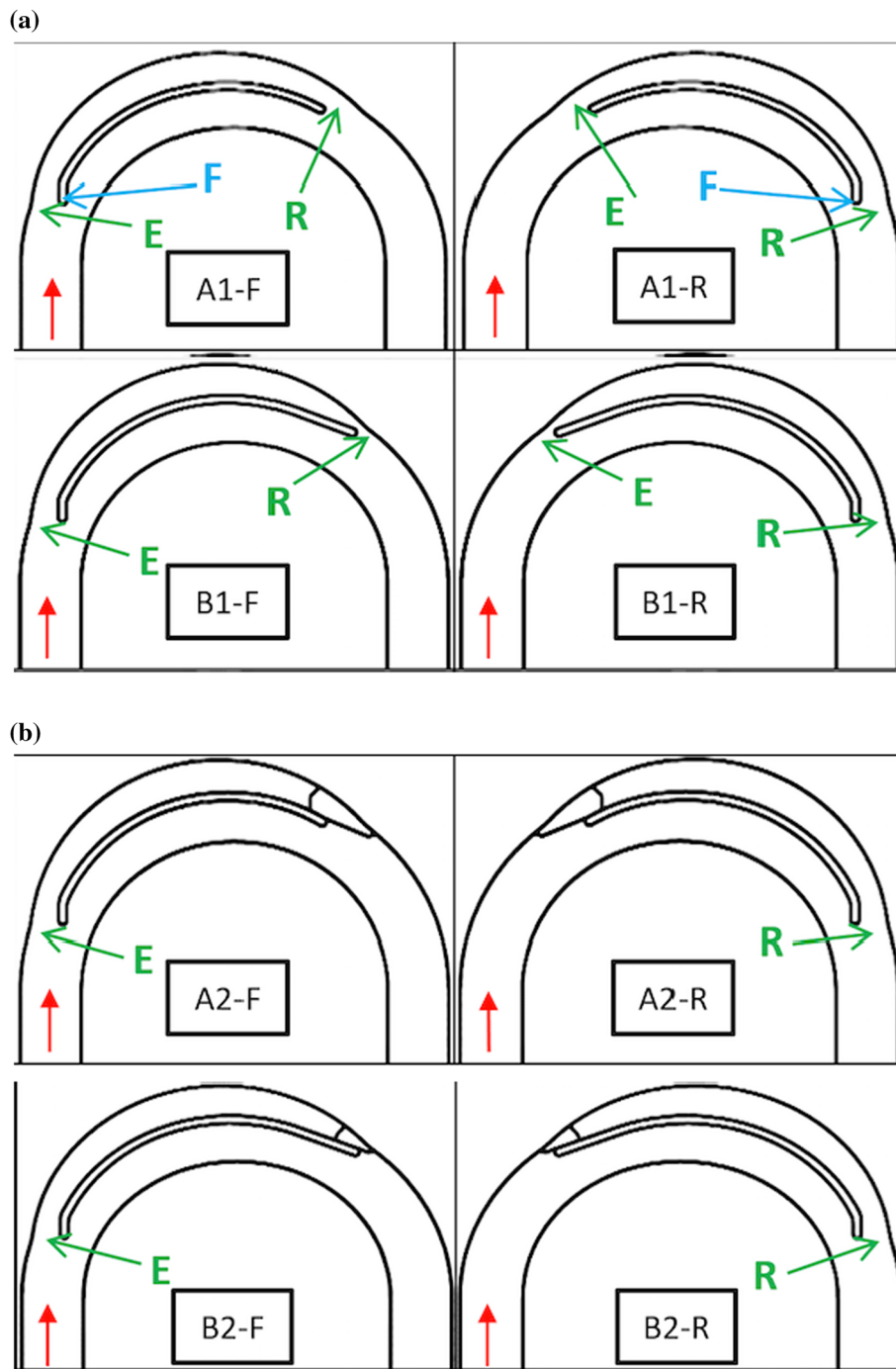
FIGURE 3. The investigated AD configurations with: (a) *patent* FL, and (b) *non-patent* FL where either its distal or proximal tear is occluded. The main flow is in the CW direction, and the FL is located at the top of the arch towards the outer wall. (E) is an entry tear, (R) is a re-entry tear, and (F) refers to the rigid flutter feature present in all cases either at the entry or re-entry tear.

non-patent (2), and its open tear with the fluttering flap was distal (R).

PIV and LIF Measurements

The laser beam from a 3 W Argon-ion laser (Laser Physics, UK) was steered and expanded through a set of mirrors and lenses into a 1 mm thick light sheet parallel to the plane of the aortic arch. It illuminated a section at mid height of the aortic conduit as shown in Fig. 1. The optical axis of a Phantom V9 CCD camera (Vision Research, USA) was set perpendicular to the plane of the aorta, and the illuminated flow was imaged at 200 fps for LIF and 1000 fps for PIV, at

$1\,\text{K} \times 1\,\text{K}$ pixel resolution. For LIF, an aqueous solution of rhodamine-B dye (Sigma Aldrich, USA) was injected at the suction side of the submerged pump as a proxy for the peripheral vein contrast media injection in CT. The Stokes-shifted optical fluorescence signal was conditioned with a long pass orange Schott glass filter before registration by the camera. Dye was injected manually with a 5 mL syringe for roughly 3 s. duration, or an average flow rate of 100 mL/min. Clinical injection rates of 200 to 300 mL/min are typical.[42] In the experimental protocol, the flow was guaranteed to equilibrate since the pump was run continuously for > 10 min before image acquisition. The camera was triggered to record the flow at the same time the dye injection was started, thus allowing the acquisition of a number of dye-free images for post processing. For the non-simultaneous PIV measurements, the flow was seeded with 5 micron TiO_2 powder (Sigma Aldrich, USA) as flow tracers. Nearly 1000 particle images were processed with the Matlab-based FFT cross correlation code PIVLAB[57] to produce 500 instantaneous velocity vector fields. The instantaneous velocity vectors were processed to produce a time-averaged field. The spatial vector resolution was approximately 1.5 mm, which was sufficient to resolve the bulk flow velocities in the FL and TL but too coarse to resolve the secondary flow features. PIV velocity uncertainty is established to be better than 5%.[46] The spatial resolution of the LIF measurements was one order of magnitude finer, which allowed the visualization of the smaller secondary flow patterns.

RESULTS

The flow in this study was steady. In the AD with *patent* FL, the effect of tear size on flow velocity is investigated using the time-averaged PIV velocity contours of Fig. 4a and the velocity statistics in Table 1. First the distal re-entry tear size effect is considered. With all else being equal, case B1F, which has a small distal reentry tear size (2.5 mm), exhibits 227% faster velocity (44.8 cm/s) in the TL than in the FL (19.7 cm/s). In case A1F which has a large distal tear (5.5 mm), the TL flow velocity (32.3 cm/s) is 51% faster than the FL flow (21.4 cm/s). Next, the effect of the proximal entry tear size is considered. In case A1R (5.5 mm proximal tear) the TL velocity (22.8 cm/s) is *23% slower* than the FL (29.7 cm/s). The opposite is true in case B1R (2.5 mm proximal tear) in which the TL velocity (41 cm/s) is *223% faster* than the FL flow (18.4 cm/s). An 2.5 mm increase in entry tear size has a significant impact on the velocity split between the TL and FL. The dissected flap position in relation to the root of the aortic arch was more proximal in A1F than

in A1R by 31 mm. Consequently, the TL:FL velocity ratio was 151% in A1F while it was only 77% in A1R, i.e. the TL flow was *faster* than the FL flow in the former model, while it was *slower* in the latter model. The overlain dashed lines on the velocity color contours mark the points where the velocity magnitudes are presented as line plots in Fig. 5a. Also cross sectional velocity profiles at the top of the aortic arch are presented in Fig. 6. The figures clearly indicate that when the entry and reentry tears are proportionally and sufficiently sized, the flow velocity in the FL is comparable to that in the TL. When their sizes are disproportionate, the smaller tear size is the limiting factor in setting the flow rate. Past the distal end of the AD flap, the TL:FL velocity disparity carries into the descending aorta giving rise to shear layer development. An example of this dynamic is shown in the LIF image of Fig. 7a where mixing layer vortices roll up just downstream of the distal end of the AD, and convect with the flow in close proximity to the outer wall of the descending aorta. From the video recording (Online Resource 1), the vortex shedding frequency was estimated to be ~ 70 Hz.

Next the flow in the *non-patent* FL cases is considered in Figs. 4b, 5b, and 6b where either the proximal tear or the distal tear is occluded. The mean flow velocity in the FL is near stagnation in the four cases. In cases A2F and A2R, the occlusion does not entirely block the AD tear allowing blood to trickle out at ~ 1 cm/s. But the nearly stagnant flow in the FL is irrespective of the occlusion affecting the proximal or the distal tear. This does not mean that dye (contrast media) does not perfuse into the FL, but it does so slowly. The LIF snapshot of Fig. 7b shows incoming dye-rich blood displacing dye-absent blood in the FL and penetrating to a certain depth into the FL before being arrested. Video recording (Online Resource 2) shows a highly dynamic and unstable vortical structure meandering in the vicinity of the proximal entry tear. It acts to intermittently draw dye-free blood from the false lumen and replace it with dye rich blood from the main aorta causing slow dye perfusion into the non-patent FL.

Next, the LIF images are interrogated as surrogates for contrast-CT radiology. They have good spatial and temporal resolution, but there are refractive laser sheet distortion artifacts as delineated in Fig. 7b. The flow front of the injected dye bolus at the time it first appears in the aorta is expected to clearly show the flow dynamics due to good brightness contrast at the interface (front) between the dye-rich and dye-poor blood. However, as seen in Fig. 8 the dye flow front is not very sharp and clean cut due to mixing taking place along the venous path from the injection site to the imaging plane. This mixing dynamic is not a focus of

FIGURE 4. Flow velocity contours in the AD with (a) patent FL, and (b) non-patent FL. Color scale is in mm/s, and flow direction is CW. Dashed lines indicate the positions where the velocity is reported as line plots in Fig. 5. Blank regions within the contours, apart from the flap itself, resulted from laser refractive distortions that prevented proper PIV analysis.

TABLE 1. Summary of the tested AD geometries.

Geometry	Patent false lumen	PT size (mm)	DT size (mm)	PT position (mm)	U_{TL} cm/s mean (SD)	U_{FL} cm/s mean (SD)
A1F	Yes	6.3	5.5	55	32.3 (5.5)	21.4 (3.9)
B1F	Yes	6.3	2.5	55	44.8 (5.1)	19.7 (4.3)
A1R	Yes	5.5	6.3	86	22.8 (3.4)	29.7 (7.1)
B1R	Yes	2.5	6.3	86	41.0 (3.7)	18.4 (10.7)
A2F	No	6.3	–	55	38.0 (9.0)	1.1 (0.5)
B2F	No	6.3	–	55	43.2 (4.1)	0.2 (0.1)
A2R	No	–	6.3	–	45.9 (11.2)	1.2 (0.8)
B2R	No	–	6.3	–	57.1 (4.7)	0.2 (0.2)

The position of the proximal tear PT is measured from the root of the ascending aorta. The velocities in the two lumens U_{TL}, U_{FL} are reported as spatial mean and spatial standard deviation computed over a flow area extending 26 mm in length, and centered at the top curvature of the aortic arch.
PT proximal tear, *DT* distal tear.

the current study. It is possible to see in the cases of Fig. 8a, that dye fills the patent FL and the TL roughly at the same rate, and the dissected flap is clearly identifiable against the backdrop of the surrounding dye. By looking at the overall aortic contrast perfusion fore and aft of the of the dissection site, there is no abrupt change in the vessel diameter in the radiographs. However, for the non-patent entry-only or reentry-only AD, the dye bolus *front* is very slow to perfuse in the FL as noted earlier in the velocity measurements, and only the TL appears in the contrast CT radiograph as shown in Fig. 8b. This causes an abrupt reduction in the aortic diameter to appear in the image coinciding with the location of the dissection, before the aortic diameter expands back to its normal size. The snapshot of Fig. 7b taken well after the injection has terminated, shows the dye had perfused a good distance into the FL making the flap and part of the FL discernible.

Quantitative LIF analysis is performed next by dividing each instantaneous image in the video sequence into approximately five zones covering the FL and TL. The spatially-averaged zonal intensity is computed at each time point to produce a time trace for the specific zone. An example is shown in Fig. 9a for case B2F. The time trace is then corrected for spatial variations in light sheet intensity according to a linear formula based on the zero-dye-concentration signal (initial part of the trace), and the fully mixed uniform-dye-concentration signal (last part of the time trace). The camera sequence started with the injection process prior to the dye reaching the aorta (zero concentration), and continued well after the injection process ended and the dye had time to complete at least two full circles in the flow loop through the pump and back. At this point it was considered nearly fully mixed (uniform concentration). The raw and corrected zonal intensity signals for case B2F are shown in Figs. 9a and 9b, respectively. This case has a proximal entry tear with no distal re-entry tear, where dye perfusion into the FL is slow. There are three salient intensity peaks at roughly 3, 9, and 15 s that correspond to three consecutive passes which the injected dye makes through the circulatory system. A complete circulation takes ~ 6 s to complete and it is characteristic of the average flow velocity (m/s) and total length of the circulatory system (m). For instance, the width of the first peak of ~ 3 s, defined by the time points where the corrected LIF intensity reaches ~ 1 a.u., is consistent with the length of the injection process. With each consecutive pass, the width of the peak increases while its intensity is reduced by 60 to 70%, by dilution with clear fluid in the tubes and reservoir. In a patient, however, dye will get diluted through excretion by the renal system and, it can also linger in crevices in the various organs.

The corrected zonal LIF signals for the *patent* FL cases B1F and B1R are presented in Fig. 10a. As the injected dye bolus reaches the clear aorta, mixing starts at the interfacial front, and the signal intensity rises fast to a peak for all zones. The peak magnitudes in the different zones are not necessarily the same because the bolus front is not a sharp interface but rather diffuse. If the injection time were sufficiently longer than 3 s, then all zonal signals would be expected to plateau to the same bolus concentration value before dropping. The rates of rise and fall of the peak are nearly similar. Towards the trailing edge of the dye bolus and from that time point onwards all zonal intensities equalize, which may be utilized as a radiological characteristic of a patent FL. The LIF signals from the other two patent cases A1F and A1R (which have larger opening tears) are not shown because they could not be linearly corrected due to the record length being cut short before reaching the fully mixed state; but the results are nearly the same as in the other patent FL cases.
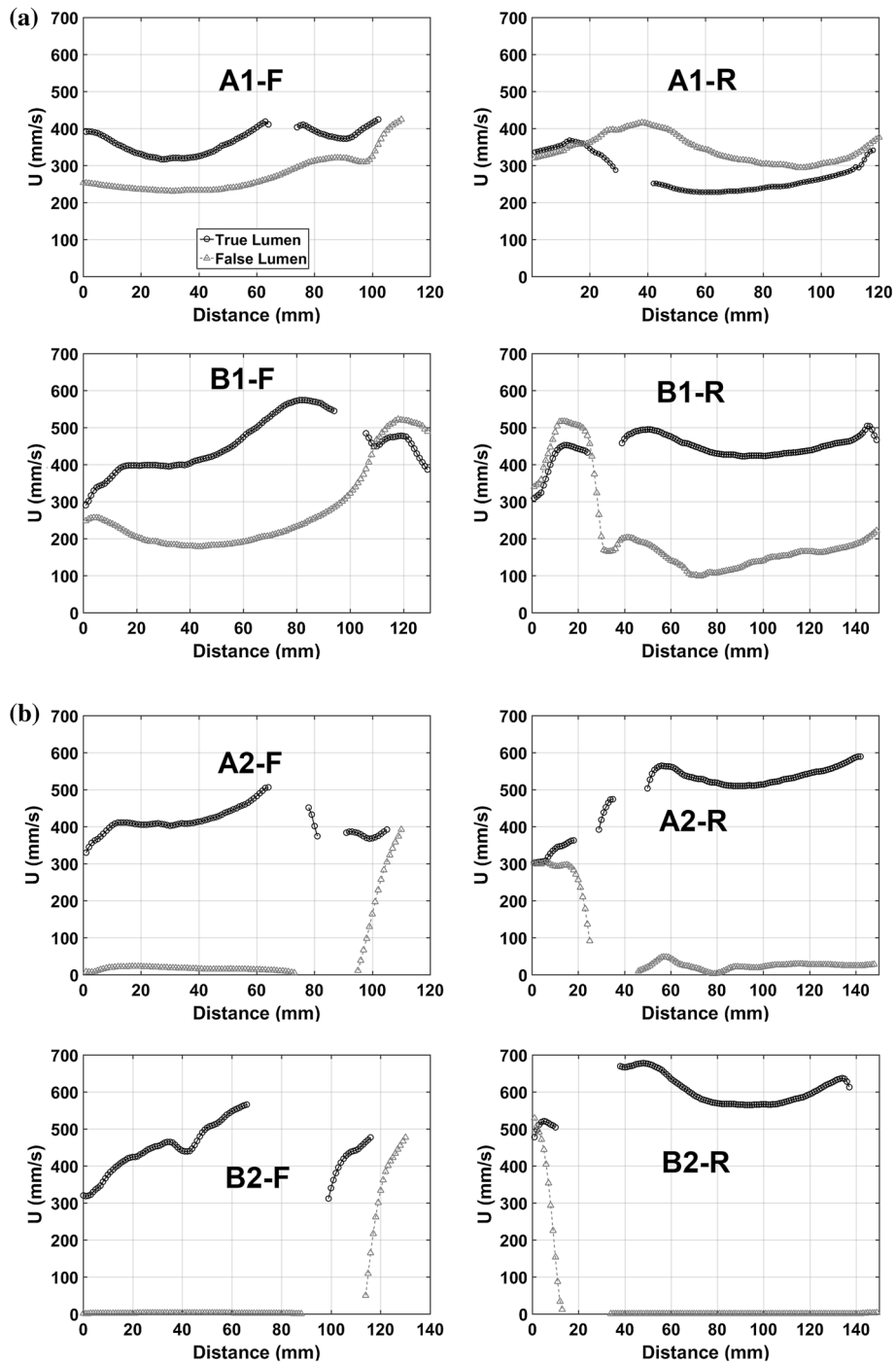
FIGURE 5. Flow velocity magnitude in the true (black line) and false (gray line) lumens for (a) the four patent FL models, and (b) the four occluded FL models along the pathlines delineated in Fig. 4.

In the *non-patent* FL scenarios A2R and A2F of Fig. 10a, the wedge blocking the respective entry or reentry tears was not perfectly seated allowing some flow to trickle as revealed in the velocity maps of Fig. 4 with noticeably increased dye perfusion in the FL compared to the fully blocked model B scenarios B2R and B2F. The FL is divided into two zones: one closer

to the open tear R3 and one farther from it R4. In cases A2F and B2F which have the distal reentry port blocked, the FL signals in the nearer zone (R3) spike with the arrival of the dye bolus nearly in sync but at a lower peak than the adjacent TL signal. Also the spike height in R3 is larger than in zone R4. Importantly, the rate of rise and fall of the peak dye concentration
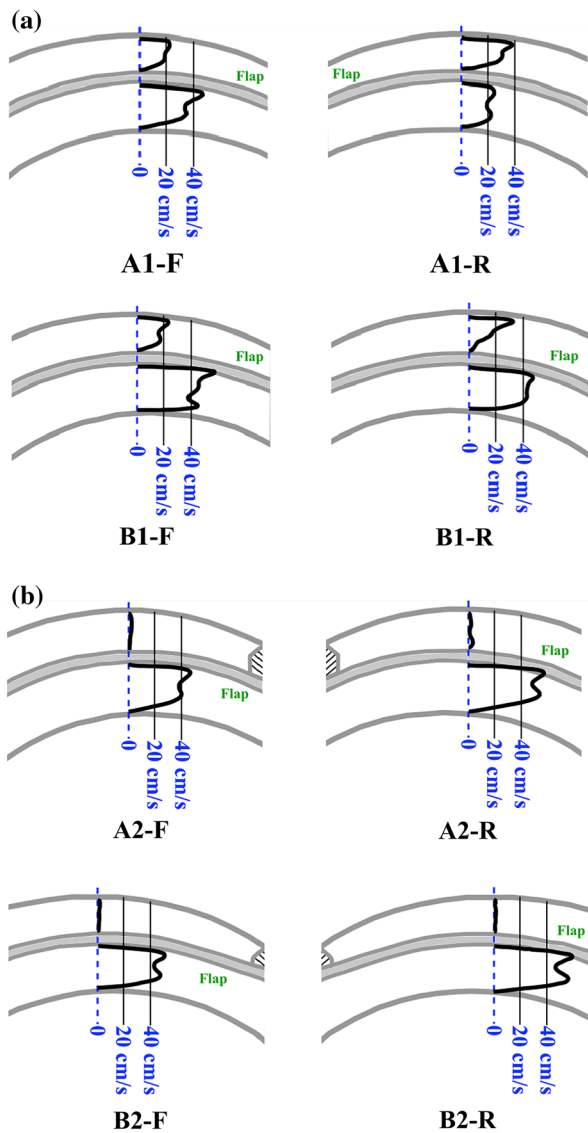
FIGURE 6. Cross sectional profiles of the streamwise velocity component taken at the top of the dissected aortic arch of Fig. 4 for (a) the four patent FL models, and (b) the four occluded FL models.
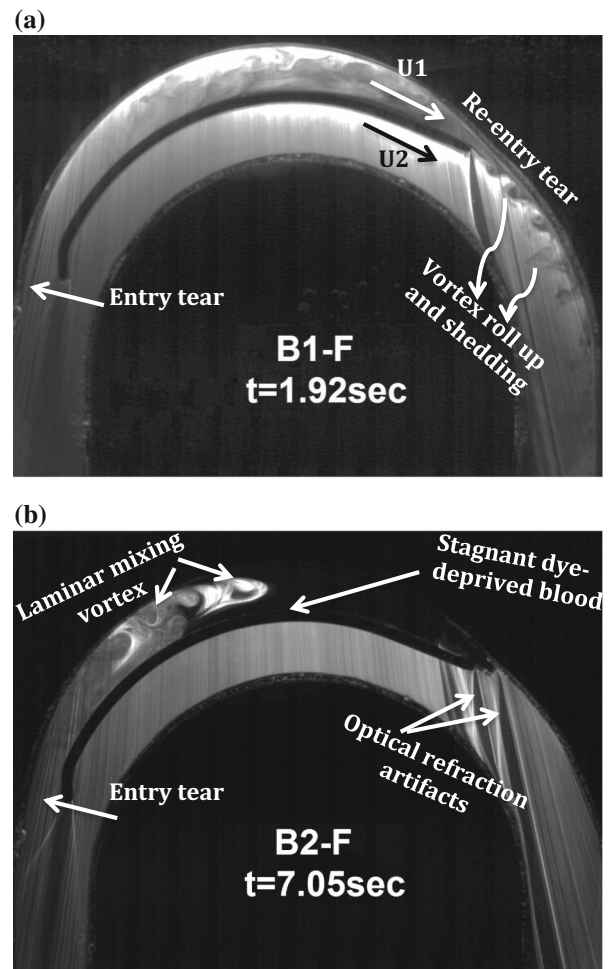

FIGURE 7. Instantaneous LIF images showing (a) the shear layer developing on the outer wall of the descending aorta in an entry-reentry type dissection; and (b) the penetration of the dye through the proximal entry tear into the stagnant FL blood. Main flow direction is CW. The time stamps correspond to the timing of Fig. 10.

signal in the TL is distinctly faster than the corresponding FL. As the dye bolus nearly clears the TL around the 4 s mark, the FL signal reaches its peak due to its much slower perfusion. The FL and TL signals do not achieve parity until the third pass. This is also noticeable in the reentry-only cases A2R and B2R.

DISCUSSION

The aim of this paper was to investigate the effect of AD disease geometry on the resulting velocity levels in the two lumina. Eight *in vitro* type-A, rigid dissection cases were investigated under steady flow conditions. The studied factors were: proximal tear location,

proximal and distal tear size, and false lumen patency. In the AD with *patent FL flow*, whether the higher velocity was skewed towards the FL or the TL depended on the entry tear proximity to the root of the aorta. When the proximal entry tear was large and close to the root of the aorta, the higher velocity manifested in the true lumen, irrespective of the distal reentry tear size. With the proximal entry tear being farther downstream and the distal entry tear being large, however, the faster velocity manifested in the FL with the larger entry tear size. The TL/FL velocity ratio was highly sensitive to the size of the entry tear, where in case A1R the ratio was 77% (< 1), and in case B1R it was 223% (> 1). Furthermore, the velocity differential across the flap resulted in shear layer vortex roll up downstream of the distal tear with a shedding frequency of 70 Hz which was comparable to the heart rate. This can be concerning if possible
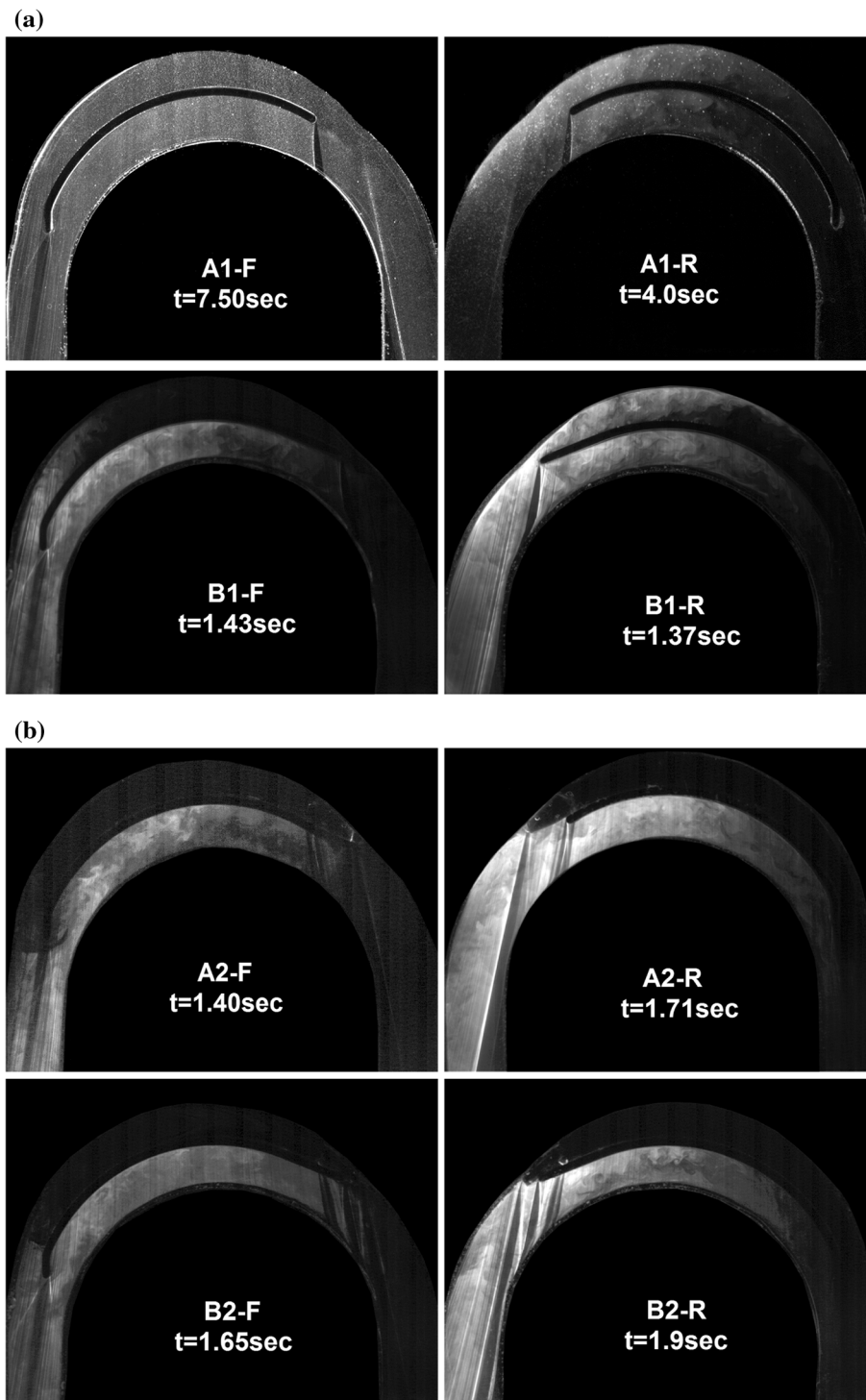
(a)

(b)

FIGURE 8. Instantaneous LIF images of the contrast bolus *flow front* for (a) the patent false lumen cases, and (b) the occluded false lumen cases. Image artifacts from laser light refraction at the proximal and distal ends of the AD septum contaminate parts of the images. The time stamps correspond to the scale in Fig. 10.

cardiac synchronization renders the shedding process more energetic. Such vortical structures, characterized by their elevated shear rate,[26,63] have been implicated in wall inflammatory degeneration and weakening.[10] They can cause pressure fluctuations, acoustic mur-murs, and the onset of turbulent flow[15] down-stream,[26,63] and wall damage and pathology.[11,64] The time-averaged flow in a *non-patent false lumen* was found to be nearly stagnant, irrespective of the entry tear being proximal or distal. A dynamic meandering

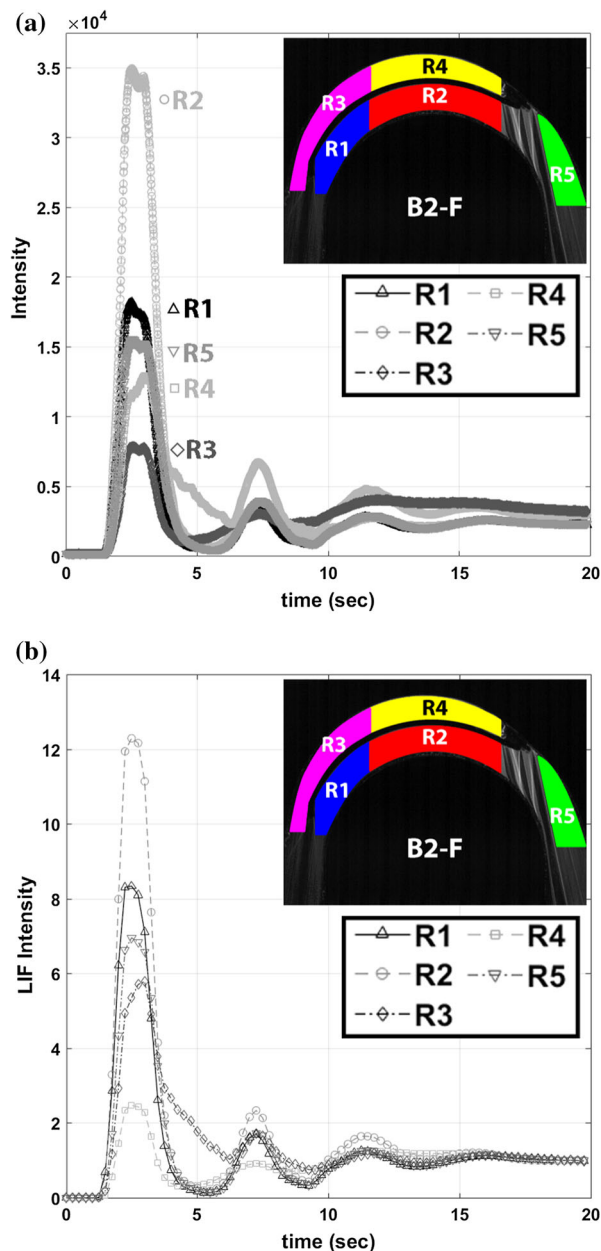BMES BIOMEDICAL ENGINEERING SOCIETY

FIGURE 9. Time trace of the spatially averaged LIF intensity in five different zones in the AD: (a) uncorrected; and (b) linear correction implemented. The LIF intensity has arbitrary units. Case B2F is used for demonstration.

to geometric configuration support this argument. Velocity can be acquired clinically using non-invasive modalities such as Doppler ultrasound and MR.[15,41]

Furthermore, the velocity measurements enlightened the interpretation of the LIF images, and the underlying perfusion of diagnostic contrast. LIF was an optical imaging surrogate for contrast-enhanced CT or MR diagnostics. The clinical diagnostic protocol starts by gaging the time it takes for a small test injection to arrive at the aorta. Image acquisition is then timed to start when the aorta is filled with the primary contrast administration. When the FL is patent, this protocol is well suited because the media perfuses at comparable rates in the two lumina. But in a non-patent FL, dye perfusion is much slower than in the TL. Under this standard imaging protocol, the contrast would fill and eventually clear the TL, without having sufficient time to perfuse through the FL. This poses a risk for a false negative diagnosis. Modified clinical imaging protocols have been proposed such as time-delayed acquisition to allow sufficient FL perfusion[13] which is supported by the LIF measurements.

There were important limitations associated with the study design including the square cross section and the planar curvature of the aorta, which were necessary for improved optical imaging. Physiologically, the aorta is round and arches in three dimensions with the flow being three dimensional and characterized by the secondary Dean vortices.[22,63] Nonetheless, these three dimensional features such as the large scale secondary Dean vortices, and the skewed velocity profile would be present in a rectangular vessel model.[6,23,31] The steady flow assumption is also a deviation, but it is an assumption frequently employed in aortic studies[38,56,63] prior to a follow-up pulsatile investigation. The rigid walls and rigid flap represent another substantial limitation. Compliance of the intimal flap is expected to have a significant role in altering the flow structures and the mixing processes; particularly that large-scale flap motion has been documented under pulsatile conditions.[7,8] The rigid vessel limits the conclusions of the study to older patients with hypertensive disease where calcification and aortic stiffening are prevalent.[9,37,40,59]

Lastly, in relation to flow measurement uncertainty, Table 1 indicates that the standard deviation to mean velocity ratio is between 10 and 25%, which is significantly higher than the expected PIV precision uncertainty of 5%.[46] Furthermore, flow rate estimates using PIV sectional velocity profiles were consistent with those from timed filling of a graduated volume, which indicated measurement bias was acceptably low.
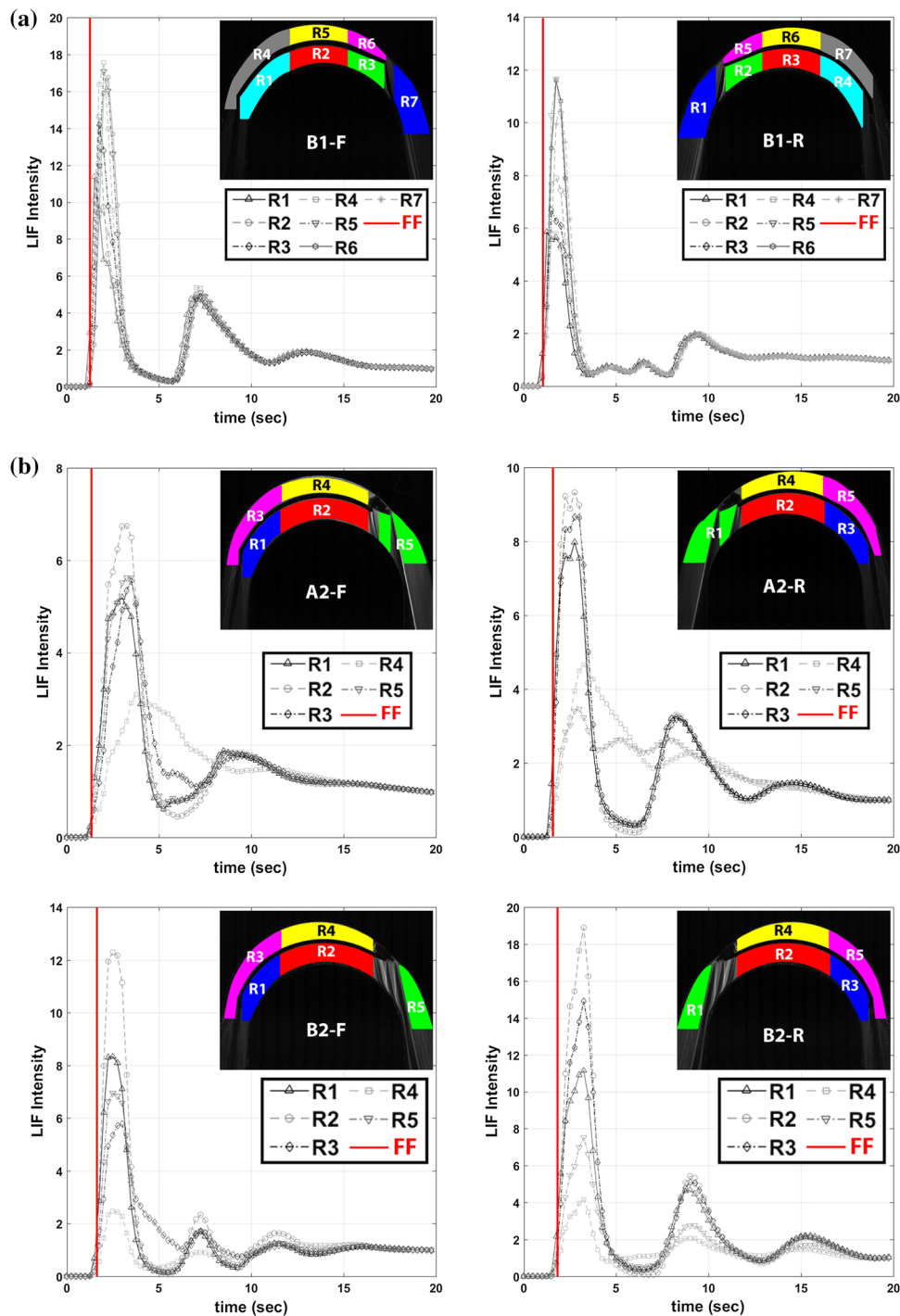
vortex structure at the entry tear generated slow blood perfusion in the FL. As suggested by Evangelista *et al.*[17] blood velocity measurements can help inform on disease progression, because noticeable vessel remodeling leading to patient complications takes about two years to manifest. Measured flow sensitivity

FIGURE 10. Time traces of the spatially averaged LIF zonal intensity (a) patent FL, and (b) non-patent FL. Vertical red line indicates the flow front time stamp corresponding to Fig. 8.

CONCLUSIONS

Whether the flow was faster in the TL or FL depended on the specific dissection geometry. In an occluded or non-patent FL, the time-averaged flow velocity was effectively zero and all the flow went through the TL. The velocity was faster in a patent FL than the TL when the proximal entry tear was located farther along the aortic arch, *and* the proximal entry tear and distal reentry tear were sufficiently large (study case A1R). This case had the highest measured FL velocity implying that the flap may be under high hemodynamic loading with risk of further tearing. The velocity pattern and magnitude in the TL/FL impacted

the type of diagnostic radiology administration protocol, which controlled the contrast perfusion rate. Delayed acquisition in diagnostic contrast-enhanced CT and MR is recommended when a non-patent FL is suspected. The results of this study bear relevance to hypertensive older patients with stiff arteries and fibrosed dissections.

ELECTRONIC SUPPLEMENTARY MATERIAL

The online version of this article (https://doi.org/10.1007/s13239-019-00407-4) contains supplementary material, which is available to authorized users.

ACKNOWLEDGMENTS

FUNDING

CONFLICT OF INTEREST

Elie Salameh declares that he has no conflict of interest. Charbel Saade has received research funding from GE healthcare USA. Ghanem Oweis declares that he has no conflict of interest.

ETHICAL APPROVAL

No human studies were carried out by the authors for this article. No animal studies were carried out by the authors for this article. No cell culture studies were carried out by the authors for this article.

REFERENCES

[1] Ab Naim, W. N., P. B. Ganesan, Z. Sun, Y. M. Liew, Y. Qian, C. J. Lee, S. Jansen, S. A. Hashim, and E. Lim. Prediction of thrombus formation using vortical structures presentation in Stanford type B aortic dissection: a preliminary study using CFD approach. *Appl. Math. Modell.* 40(4):3115–3127, 2016.

[2] Abbas, A., I. W. Brown, C. R. Peebles, S. P. Harden, and J. S. Shambrook. The role of multidetector-row CT in the diagnosis, classification and management of acute aortic syndrome. *Br. J. Radiol.* 87(1042):20140354, 2014.

[3] Ahmed, S. B., D. Dillon-Murphy, and C. A. Figueroa. Computational study of anatomical risk factors in idealized models of type B aortic dissection. *Eur. J. Vasc. Endovasc. Surg.* 52(6):736–745, 2016.

[4] Alloush, M. M., G. F. Oweis, and R. Nasr. Computational study of anatomical risk factors in idealized models of type B aortic dissection. *Eur. J. Vasc. Endovasc. Surg.* 52(6):736–745, 2016.

[5] Asouhidou, I., and T. Asteri. Acute aortic dissection: be aware of misdiagnosis. *BMC Res. Notes* 2(1):25, 2009.

[6] Berger, S. A., L. Talbot, and L. S. Yao. Flow in curved pipes. *Annu. Rev. Fluid Mech.* 15(1):461–512, 1983.

[7] Birjiniuk, J., L. H. Timmins, M. Young, B. G. Leshnower, J. N. Oshinski, D. N. Ku, and R. K. Veeraswamy. Pulsatile flow leads to intimal flap motion and flow reversal in an in vitro model of type B aortic dissection. *Cardiovasc. Eng. Technol.* 8(3):378–389, 2017.

[8] Canchi, S., X. Guo, M. Phillips, Z. Berwick, J. Kratzberg, J. Krieger, B. Roeder, S. Haulon, S. Chambers, and G. S. Kassab. Role of re-entry tears on the dynamics of type B dissection flap. *Ann. Biomed. Eng.* 46(1):186–196, 2018.

[9] Cavalcante, J. L., J. A. C. Lima, A. Redheuil, and M. H. Al-Mallah. Aortic stiffness: current understanding and future directions. *J. Am. Coll. Cardiol.* 57(14):1511–1522, 2011.

[10] Cebral, J., E. Ollikainen, B. J. Chung, F. Mut, V. Sippola, B. R. Jahromi, R. Tulamo, *et al.* Flow conditions in the intracranial aneurysm lumen are associated with inflammation and degenerative changes of the aneurysm wall. *Am. J. Neuroradiol.* 38:119, 2016.

[11] Cecchi, E., C. Giglioli, S. Valente, C. Lazzeri, G. F. Gensini, R. Abbate, and L. Mannini. Role of hemodynamic shear stress in cardiovascular disease. *Atherosclerosis* 214(2):249–256, 2011.

[12] Cheng, Z., F. P. P. Tan, C. V. Riga, C. D. Bicknell, M. S. Hamady, R. G. J. Gibbs, N. B. Wood, and X. Y. Xu. Analysis of flow patterns in a patient-specific aortic dissection model. *J. Biomech. Eng.* 132(5):051007, 2010.

[13] Clough, R. E., T. Hussain, S. Uribe, G. F. Greil, R. Razavi, P. R. Taylor, T. Schaeffter, and M. Waltham. A new method for quantification of false lumen thrombosis in aortic dissection using magnetic resonance imaging and a blood pool contrast agent. *J. Vasc. Surg.* 54(5):1251–1258, 2011.

[14] Clough, R. E., M. Waltham, D. Giese, P. R. Taylor, and T. Schaeffter. A new imaging method for assessment of aortic dissection using four-dimensional phase contrast magnetic resonance imaging. *J. Vasc. Surg.* 55(4):914–923, 2012.

[15] Dyverfeldt, P., J. P. Kvitting, A. Sigfridsson, J. Engvall, A. F. Bolger, and T. Ebbers. Assessment of fluctuating velocities in disturbed cardiovascular blood flow: in vivo feasibility of generalized phase-contrast MRI. *J. Magn. Reson. Imaging: Off. J. Int. Soc. Magn. Reson. Med.* 28(3):655–663, 2008.

[16] Endo, S., H. L. Goldsmith, and T. Karino. Flow patterns and preferred sites of atherosclerotic lesions in the human aorta–I. Aortic arch. *Biorheology* 51(4–5):239–255, 2014.

[17] Evangelista, A., A. Salas, A. Ribera, I. Ferreira-González, H. Cuellar, V. Pineda, T. González-Alujas, B. Bijnens, G.

Permanyer-Miralda, and D. Garcia-Dorado. Long-term outcome of aortic dissection with patent false lumen: predictive role of entry tear size and location. *Circulation* 125:3133, 2012.

[18]Fojtik, J. P., T. G. Costantino, and A. J. Dean. The diagnosis of aortic dissection by emergency medicine ultrasound. *J. Emerg. Med.* 32(2):191–196, 2007.

[19]Golledge, J., and K. A. Eagle. Acute aortic dissection. *Lancet* 372(9632):55–66, 2008.

[20]Hatzaras, I., M. Tranquilli, M. Coady, P. M. Barrett, J. Bible, and J. A. Elefteriades. Weight lifting and aortic dissection: more evidence for a connection. *Cardiology* 107(2):103–106, 2007.

[21]Hayter, R. G., J. T. Rhea, A. Small, F. S. Tafazoli, and R. A. Novelline. Suspected aortic dissection and other aortic disorders: multi–detector row CT in 373 cases in the emergency setting. *Radiology* 238(3):841–852, 2006.

[22]Hellström, L. H., M. B. Zlatinov, G. Cao, and A. J. Smits. Turbulent pipe flow downstream of a 90° bend. *J. Fluid Mech.* 2013. https://doi.org/10.1017/jfm.2013.534.

[23]Hille, P., R. Vehrenkamp, and E. O. Schulz-Dubois. The development and structure of primary and secondary flow in a curved square duct. *J. Fluid Mech.* 151:219–241, 1985.

[24]Hope, T. A., M. Markl, L. Wigström, M. T. Alley, D. C. Miller, and R. J. Herfkens. Comparison of flow patterns in ascending aortic aneurysms and volunteers using four-dimensional magnetic resonance velocity mapping. *J. Magn. Reson. Imaging* 26(6):1471–1479, 2007.

[25]Husainy, M. A., F. Sayyed, and S. Puppala. Acute aortic syndrome—pitfalls on gated and non-gated CT scan. *Emerg. Radiol.* 23(4):397–403, 2016.

[26]Karasso, P. S., and M. G. Mungal. Scalar mixing and reaction in plane liquid shear layers. *J. Fluid Mech.* 323:23–63, 1996.

[27]Karmonik, C., J. Bismuth, D. J. Shah, M. G. Davies, D. Purdy, and A. B. Lumsden. Computational study of haemodynamic effects of entry-and exit-tear coverage in a DeBakey type III aortic dissection: technical report. *Eur. J. Vasc. Endovasc. Surg.* 42(2):172–177, 2011.

[28]Karmonik, C., S. Partovi, M. Müller-Eschner, J. Bismuth, M. G. Davies, D. J. Shah, M. Loebe, D. Böckler, A. B. Lumsden, and H. von Tengg-Kobligk. Longitudinal computational fluid dynamics study of aneurysmal dilatation in a chronic DeBakey type III aortic dissection. *J. Vasc. Surg.* 56(1):260–263, 2012.

[29]Khanafer, K., and R. Berguer. Fluid–structure interaction analysis of turbulent pulsatile flow within a layered aortic wall as related to aortic dissection. *J. Biomech.* 42(16):2642–2648, 2009.

[30]Knollmann, F. D., J. M. Lacomis, I. Ocak, and T. Gleason. The role of aortic wall CT attenuation measurements for the diagnosis of acute aortic syndromes. *Eur. J. Radiol.* 82(12):2392–2398, 2013.

[31]Krishna, C. V., N. Gundiah, and J. H. Arakeri. Separations and secondary structures due to unsteady flow in a curved pipe. *J. Fluid Mech.* 815:26–59, 2017.

[32]Ku, D. N. Blood flow in arteries. *Annu. Rev. Fluid Mech.* 29(1):399–434, 1997.

[33]Kurabayashi, M., N. Miwa, D. Ueshima, K. Sugiyama, K. Yoshimura, Ta Shimura, H. Aoyagi, K. Azegami, K. Okishige, and M. Isobe. Factors leading to failure to diagnose acute aortic dissection in the emergency room. *J. Cardiol.* 58(3):287–293, 2011.

[34]Kurabayashi, M., K. Okishige, D. Ueshima, K. Yoshimura, T. Shimura, H. Suzuki, A. Mitsutoshi, H. Aoyagi, Y.

Otani, and M. Isobe. Diagnostic utility of unenhanced computed tomography for acute aortic syndrome. *Circ. J.* 78(8):1928–1934, 2014.

[35]Le Blanc-Louvry, I., S. Thureau, K. Ledoux, B. Mogdad, E. Lagroy, J. N. Dacher, and G. Tournel. False positive aortic dissection on postmortem computed tomography. *Forensic Sci. Int.* 254:e4–e6, 2015.

[36]Ledneva, E., S. Karie, V. Launay-Vacher, N. Janus, and G. Deray. Renal safety of gadolinium-based contrast media in patients with chronic renal insufficiency 1. *Radiology* 250(3):618–628, 2009.

[37]Lee, H.-Y., and O. Byung-Hee. Aging and arterial stiffness. *Circ. J.* 74(11):2257–2262, 2010.

[38]Liu, X., P. Fang, Y. Fan, X. Deng, D. Li, and Sh Li. A numerical study on the flow of blood and the transport of LDL in the human aorta: the physiological significance of the helical flow in the aortic arch. *Am. J. Physiol. Heart Circ. Physiol.* 297(1):H163–H170, 2009.

[39]Liu, Q., J. P. Lu, F. Wang, L. Wang, and J. M. Tian. Three-dimensional contrast-enhanced MR angiography of aortic dissection: a pictorial essay. *Radiographics* 27(5):1311–1321, 2007.

[40]London, G. M., and A. P. Guerin. Influence of arterial pulse and reflected waves on blood pressure and cardiac function. *Am. Heart J.* 138(3):S220–S224, 1999.

[41]Markl, M., P. J. Kilner, and T. Ebbers. Comprehensive 4D velocity mapping of the heart and great vessels by cardiovascular magnetic resonance. *J. Cardiovasc. Magn. Reson.* 13(1):7, 2011.

[42]McMahon, M. A., and C. A. Squirrell. Multidetector CT of aortic dissection: a pictorial review. *Radiographics* 30(2):445–460, 2010.

[43]Nagpal, P., A. Khandelwal, S. S. Saboo, G. Bathla, M. L. Steigner, and F. J. Rybicki. Modern imaging techniques: applications in the management of acute aortic pathologies. *Postgrad. Med. J.* 91:449, 2015.

[44]Nagra, K., R. Coulden, and M. S. McMurtry. A type A aortic dissection missed by non-cardiac gated contrast-enhanced computed tomography due to an aortic root dissection flap masquerading as an aortic valve apparatus: a case report. *J. Med. Case Rep.* 7(1):285, 2013.

[45]Neema, P Kumar. Acute aortic dissection: pitfalls in the diagnosis. *Ann. Card. Anaesth.* 16(2):83, 2013.

[46]Oweis, G. F., and S. L. Ceccio. Instantaneous and time-averaged flow fields of multiple vortices in the tip region of a ducted propulsor. *Exp. Fluids* 38(5):615–636, 2005.

[47]Raymond, C. E., B. Aggarwal, P. Schoenhagen, D. M. Kralovic, K. Kormos, D. Holloway, and V. Menon. Prevalence and factors associated with false positive suspicion of acute aortic syndrome: experience in a patient population transferred to a specialized aortic treatment center. *Cardiovasc. Diagn. Ther.* 3(4):196, 2013.

[48]Rinaudo, A., G. D'Ancona, J. J. Lee, G. Pilato, A. Amaducci, R. Baglini, F. Follis, M. Pilato, and S. Pasta. Predicting outcome of aortic dissection with patent false lumen by computational flow analysis. *Cardiovasc. Eng. Technol.* 5(2):176–188, 2014.

[49]Rindt, C. C. M., A. A. Van Steenhoven, J. D. Janssen, and G. Vossers. Unsteady entrance flow in a 90 curved tube. *J. Fluid Mech.* 226:445–474, 1991.

[50]Rudenick, P. A., B. H. Bijnens, D. García-Dorado, and A. Evangelista. An in vitro phantom study on the influence of tear size and configuration on the hemodynamics of the lumina in chronic type B aortic dissections. *J. Vasc. Surg.* 57(2):464–474, 2013.

[51]Saade, C., R. Bourne, M. Wilkinson, M. Evanoff, and P. Brennan. A reduced contrast volume acquisition regimen based on cardiovascular dynamics improves visualisation of head and neck vasculature with carotid MDCT angiography. *Eur. J. Radiol.* 82(2):e64–e69, 2013.

[52]Salvolini, L., P. Renda, D. Fiore, M. Scaglione, G. P. Piccoli, and A. Giovagnoni. Acute aortic syndromes: role of multi-detector row CT. *Eur. J. Radiol.* 65(3):350–358, 2008.

[53]Shi, Y., Y. M. Zhu, Hua Q Chang, and Y. Liu. The risk of stanford type-A aortic dissection with different tear size and location: a numerical study. *Biomed. Eng. Online* 15(2):128, 2016.

[54]Siegal, E. M. Acute aortic dissection. *J. Hosp. Med.* 1(2):94–105, 2006.

[55]Soudah, E., P. Rudenick, M. Bordone, B. Bijnens, D. García-Dorado, A. Evangelista, and E. Oñate. Validation of numerical flow simulations against in vitro phantom measurements in different type B aortic dissection scenarios. *Comput. Methods Biomech. Biomed. Eng.* 18(8):805–815, 2015.

[56]Stevens, M. C., F. M. Callaghan, P. Forrest, P. G. Bannon, and S. M. Grieve. Flow mixing during peripheral veno-arterial extra corporeal membrane oxygenation–a simulation study. *J. Biomech.* 55:64–70, 2017.

[57]Thielicke, W., and E. Stamhuis. PIVlab–towards user-friendly, affordable and accurate digital particle image velocimetry in MATLAB. *J. Open Res. Softw.* 2(1):30, 2014.

[58]Tsai, T. T., A. Evangelista, C. A. Nienaber, T. Myrmel, G. Meinhardt, J. V. Cooper, D. E. Smith, *et al.* Partial thrombosis of the false lumen in patients with acute type B aortic dissection. *N. Engl. J. Med.* 357(4):349–359, 2007.

[59]Tsai, T. T., M. S. Schlicht, K. Khanafer, J. L. Bull, D. T. Valassis, D. M. Williams, Ramon Berguer, and K. A. Eagle. Tear size and location impacts false lumen pressure in an ex vivo model of chronic type B aortic dissection. *J. Vasc. Surg.* 47(4):844–851, 2008.

[60]Tsai, T. T., S. Trimarchi, and C. A. Nienaber. Acute aortic dissection: perspectives from the international registry of acute aortic dissection (IRAD). *Eur. J. Vasc. Endovasc. Surg.* 37(2):149–159, 2009.

[61]Tse, K. M., P. Chiu, H. P. Lee, and P. Ho. Investigation of hemodynamics in the development of dissecting aneurysm within patient-specific dissecting aneurismal aortas using computational fluid dynamics (CFD) simulations. *J. Biomech.* 44(5):827–836, 2011.

[62]Vantine, P. R., J. K. Rosenblum, W. G. Schaeffer, K. T. Williams, D. W. Dockray, J. M. Levsky, L. B. Haramati, and L. H. Ketai. Can non-contrast-enhanced CT (NECT) triage patients suspected of having non-traumatic acute aortic syndromes (AAS)? *Emerg. Radiol.* 22(1):19–24, 2015.

[63]Zhu, C., J.-H. Seo, and Rajat Mittal. Computational modelling and analysis of haemodynamics in a simple model of aortic stenosis. *J. Fluid Mech.* 851:23–49, 2018.

[64]Ziegler, M., J. Lantz, T. Ebbers, and P. Dyverfeldt. Assessment of turbulent flow effects on the vessel wall using four-dimensional flow MRI. *Magn. Reson. Med.* 77(6):2310–2319, 2017.